IIETA International Information and Engineering Technology Association
Advancing the World of Information and Engineering

Mathematical Modelling of Engineering Problems
Vol. 12, No. 4, April, 2025, pp. 1101-1114
Journal homepage: http://iieta.org/journals/mmep

A Simplified Analytical Model for Radiant Panel Temperature with Variable Heat Sink

Hasanain J.A. Juaifer*, Jaafar Ali Mahdi, Ali A. Abdulrasool

Department of Mechanical Engineering, College of Engineering, University of Kerbala, Karbala 56001, Iraq

Corresponding Author Email: hassanen.j@uokerbala.edu.iq

https://doi.org/10.18280/mmep.120402

Received: 12 November 2024
Revised: 15 January 2025
Accepted: 24 January 2025
Available online: 30 April 2025

Keywords:
radiant cooling panel (RCP), separation of variable, discontinuous temporal method, numerical simulation for RCP

ABSTRACT

The radiant panel has gained attention due to its versatility in both structural applications and energy requirements. However, limited research has focused on wall panels and their performance with variable energy sources. This study presents a new mathematical model designed to improve the thermal performance prediction of radiant wall panels. The model utilizes the method of separation of variables to address a discontinuous, time-dependent heat sink represented as a Heaviside step function. Subsequently, the differential equation governing two-dimensional heat conduction in a panel containing a serpentine tube is solved. Analytical solutions are pursued for both steady and unsteady conditions, and the findings are compared with experimental results and simulations conducted using ANSYS-Fluent. Our analysis reveals that keeping a constant water inlet temperature and increasing the flow rate leads to a significant 76.7% temperature reduction. Additionally, changing the tube diameter and adjusting the panel's aspect ratio result in temperature differentials decreasing by 83% and 70%. Increasing the aspect ratio by two enhances heat removal efficiency by around 0.6%.

1. INTRODUCTION

Human body temperature is generally influenced by the environment, and the body's response to that effect depends on a number of variables. This exchange of energy between individuals and their surroundings is most often due to radiation. The latter is an energy transmission via electromagnetic waves that occur everywhere, especially in relatively large areas. Nowadays, traditional air conditioning systems mainly regulate the sensible temperature, humidity, and ventilation amounts in the target space. However, the parameter, also known as a mean radiant temperature, or MRT, is usually not accounted. Other systems, though, those incorporate the radiation with air conditioning process such as radiant heating/cooling panels, or RCPs, can be more preferable due to their advantages in thermal comfort.

These RCPs are very adaptable to most building designs and layouts, thus they may be retrofitted into existing structures or installed in a new construction. Also, they use less energy than the conventional air conditioning systems and generate less noise pollution, since they do not rely on forced air, which can disperse allergens and contaminants throughout the space [1]. In addition, they may be fueled by renewable energy sources such as solar or geothermal energy, which further reduces their environmental effect. With radiant cooling panel, chilled water is pumped via pipes implanted in building's walls. The pipes may be mounted on surfaces, or they can be embedded into the walls. When cold water flows through the system, it absorbs heat from the panel and cools its wall surface. This treated surface subsequently emits cool energy to the room's inhabitants, providing a pleasant and conditioned interior. Additionally, the chilled surfaces handle a sizable volume of air, which enhances the comfort of the interior environment even more. The low exergy destruction characteristics of radiant systems may allow for a more comfortable living environment, according to the study conducted by Koca [2]. Reducing free convective heat transfer, which is a primary source of discomfort in living spaces, and boosting radiative heat transfer can be done by arranging the large surfaces as heat sources or sinks. The three main types are radiant ceiling, floor, and wall panel systems. The question is which side of the room would be ideal for installing the radiant panel. The popular positions are used to be on the floor and/or ceiling. Others, though, believe that walls or windows can also be effective. However, for any form of this air conditioning system, numerous works were accomplished. Possibly, beginning with the review papers can give a complete survey for this subject.

1.1 General surveys

Krajčík et al. [3] provided an overview of the possible benefits and disadvantages of radiant wall against radiant ceiling and floor systems. The study demonstrated that, when correctly planned and implemented, radiant wall panels paired with low-grade energy sources may provide cost-effective and environmentally friendly heating systems. Furthermore, radiant wall panels are easier to install than radiant ceiling and floor ones, which could result in energy savings under certain conditions. In the research of Karakoyun et al. [4], sidewalls

served as heat sinks to ease the summertime circumstances that can develop when building's walls are inadequately insulated or exposed to solar radiation. Convective and radiative heat fluxes were computed. A hydraulic radiant sub-floor was found to have a large heat transfer boost from 3% to 5%. A heated floor has a higher overall heat transfer coefficient than the colder one because of stronger air movements. This is due to the tendency of air molecules over a hot floor to rise due to buoyant forces outweighing gravity forces. The average efficiency of a radiation-based cooling system was 91% for all treated floors. The researchers Krajčík and Šikula [5] identified and directly compared four different types of wall cooling systems, three of which can be retrofitted into existing buildings. It is demonstrated how multiple configurations of pipe placement, material layers, and core thermal conductivity enable compromise between the various performance indicators to construct a system with desired specifications. According to the study of Koca et al. [6], radiant wall applications have become more popular than floor and ceiling ones because of their benefits, although there had never been any experimental studies on radiant wall cooling before. Radiative and convective heat transfer accounted for, respectively, 67% and 33% of the total heat transfer when a radiant wall cooling panel was considered.

Conroy and Mumma [7] presented an overview of the fundamental heat transfer equations used to calculate the mean temperature of radiant cooling panel as a function of panel's design, material, flow rate, coolant temperature, and space temperature. The design issue, they said, is to ascertain the mean panel temperature for a particular mass flow rate and geometry. A complete review by Hassan and Abdelaziz [8] revealed that the majority of research within reach noted that radiant systems perform better than all other devices if the temperature of the chilled water is low enough with affordable surface condensation. For a better explanation of the dynamic cooling properties of radiant panel systems, they found that transient mathematical models should be created to replace the widely utilized steady-state models. Also, for radiant systems to operate in both heating and cooling modes, sophisticated control strategies are necessary. Finally, to assess the effect of chilled water tube arrangement, tube diameter, and tube spacing on the temperature uniformity of thermally activated slabs, design formulas are needed. Hu et al. [9] summarized works on radiant cooling systems, including those on radiant system conduction, cooling loads, cooling capacity, heat transfer coefficients of cooling surfaces, thermal performance of buildings, and radiant system control strategy. The aim was to provide a scientific support for passive cooling building solutions, thermal performance optimization, and radiant cooling system design. Because of the thermal mass surrounding the hydraulic pipes, the direct heat transfer of cooling surfaces was not similar to that removed by the internal water systems.

1.2 Previous experiments

There are studies that included real-scale data. For illustration, a real hospital room was selected for the cooling ceiling system by Fonseca [10]. The thermal efficiency of the cooling device was acquired by the temperature variations while the circuit's overall pressure drop was estimated from water flow rates. For the six tests with water supply temperatures changing from 11.4°C to 17.7°C, a correlation between the thermal power and average surface temperature was developed. In the study of Seyam et al. [11], several sizes and locations of full-scale room models were simulated to examine heating panels. The accuracy of the numerical technique was confirmed by experimental measurements. They found that the location of the heater influenced the temperature distribution, and it was reported that the heater surface temperature should not exceed 29°C to ensure a thermal comfort when the inside air temperature was 23°C. The investigator Koca et al. [6] conducted a number of tests to assess the hydronic radiant wall cooling system's capabilities. To obtain realistic results, the radiant wall's convective, radiative, and total heat transfer coefficients were measured in a climatic test chamber. The mean values of these coefficients were 8.25, 5.52, and 2.41 $W/m^2.K$, respectively. Radiation was responsible for 70% of the total heat transfer on average. The cooling capacity of the panel with aluminum conductive layer was around 21% more than that of the traditional panel. The experimental and numerical study of Çolak et al. [12] dealt with the shortcomings of radiant-cooled wall devices. The convection, radiation, and total heat transfer coefficients were computed using seven different artificial neural network models.

In order to achieve more cost and performance improvements, radiant systems have been integrated with other passive methods. The study that was published by Shen et al. [13] explored the use of a ground-source heat exchanger and glass box with embedded pipe as a direct use of natural energy for winter heating. Numerical analyses of heat and fluid flow were additionally performed for the pipe implanted in the window. The system's effectiveness was evaluated using ground-source water at varied water flow rates and outside temperatures. Hot water was used to warm the window, which is usually cooler than the room temperature. Thus, in the winter, a greater proportion of natural resources can be used efficiently because these sources like the ground are sufficient to reduce the heating burden. The investigators Jiang et al. [14] introduced their innovative refrigerant-direct radiant cooling system (RDRC) to the field. The terminal surface temperature of the RDRC was uniformly distributed, and the system was very effective. According to the findings, the aspect ratio of 0.88, copper pipe diameter of 6.0 mm, copper pipe spacing of 40.0 mm, and fin height of 40.0 mm were all recommended. Following Radzai et al. [15], the elevated risk of surface condensation is the reason why radiant cooling is occasionally used in hot and humid conditions. Surface condensation is less likely to occur when the supply water temperature is higher than the dew point of indoor air. However, the radiant panel system will not work to its fullest capacity if the supply water temperature is increased. They concluded that the flow is crucial to maximizing the cooling capacity of the system. The optimal goals for these systems also include reducing pressure drop, raising cooling capacity, and adjusting temperature homogeneity.

1.3 Other approaches

A considerable amount of studies has also been devoted to numerical and theoretical methods. Jeong and Mumma [16] used panel performance data generated by a verified analytical model to statistically quantify the impact of various design factors and their combinations on the panel cooling capacity. The model, which was a first order linear equation, was for both natural and mixed convection conditions. A brand-new semi-analytical numerical model was developed by Tye-

Gingras and Gosselin [17] in order to calculate the temperature field and steady-state heat transfer of such panels. The model was then compared to the entirely analytical one that ASHRAE advised. The analytical model was satisfactory and accurate but not particularly flexible because the tube spacing, heat transfer coefficient, and fin efficiency must remain constant across the whole tubing length for the methodology to be applicable. Shin et al. [18] conducted theoretical research to assess the relationship between heat flux and design factors using the calculation method from the ASHRAE Handbook. Graphic charts were made to help designers take into consideration during the design stage: Heat flux, difference between the maximum and minimum floor surface temperatures, and the maximum floor surface temperature.

By using theoretical and numerical data, Acikgoz and Kincay [19] found that the radiative to convective heat transfer coefficients are ranged from 0.88 to 1.79. Novel correlations for the radiative heat-transfer coefficient and ratio of the radiative to convective heat-transfer coefficients were also created for walls cooled by radiation. Various room sizes, emissivity ratings, and temperature ranges were tested. In Acikgoz and Kincay [19]'s work, the engineering equation solver (EES) was used to examine the total and radiative heat transfer rates in an enclosure heated from a single wall at different surface emissivities. They showed that the average radiative coefficient, ranged between 5.4 and 5.5 $W/m^2.K$, slowly varies with room size. They claimed that the overall heat transfer coefficient is between 10.2 and 10.8 $W/m^2.K$ for an emissivity value of 0.9. The average radiation to total heat transfer ratio was found to be between 64 and 67 percent. Su et al. [20] developed a two-dimensional mathematical model of steady state heat transfer using the finite difference technique. The surface and internal temperatures of the concrete panel were focused on during the numerical modeling. It was noticed that the concrete panel's thermal inertia constantly lowers the temperature of the panel.

To explore further related works to the current, Zhang et al. [21] has created a mathematical model for unsteady state heat transport. The indoor parameters during the summertime were examined, and the findings showed that the ceiling surface's temperature dropped quickly after the startup period. The radiant heat flux, however, from the ceiling decreased swiftly to a low point before slowly climbing back to a steady state. When subjected to heat flux from the bottom through convection and radiation, the flow passage designs had an impact on how well the panel performs in the steady state. They demonstrated how the panel aspect ratio should be altered to promote more uniform panel temperature distribution and save pumping power. A simplified model for top-insulated metal ceiling radiant cooling panels with serpentine tube arrangement was produced in the study of Yu et al. [22], in order to anticipate mainly the output water temperature and cooling capacity. The simplified model assumed thermal symmetry and ignored the edges of the semi-circular tubes. The results showed that (1) the tube spacing has a significant effect on cooling capacity within the useful range of tube spacing from 0.05 to 0.3 m, (2) the tube thermal conductivity has a significant effect on cooling capacity if it is less than 1.0 W/m.K, (3) the panel thickness has a significant effect on cooling capacity if it is less than 0.5 mm, and (4) the water flowrate should be sufficient to keep the flow in turbulent regime. To analyze certain floor heating system parameters, Oubenmoh et al. [23] performed simulations for design optimization. They investigated several under-floor heating configurations using a two-dimensional simulation model. Analyses were conducted on three patterns including, serpentine, counter flow spiral, and modulated spiral. The main findings revealed that the stream velocity does not considerably influence the thermal behavior of the under-floor heating system. Thus, by reducing the water inlet velocity, the energy consumption of the pump can be decreased, but additional piping diameter considerations are required. Also, the temperature of the incoming water has a major effect on the heating time. Ultimately, more optimization is needed to reduce the amount of energy used for heating.

The performance of a radiant panel containing serpentine tube arrangement was investigated by Mosa et al. [24] with aspect ratio between 0.24 and 2.79. It was found that the aspect ratio of 1.05 pertains to more energy efficient panel. The paper of Qin et al. [25] offered a simplified model and anticipated cooling load based on the concept of human thermal comfort. The relationships between design, operating, and thermal comfort characteristics were investigated using simulations. According to the findings, the radiant surface temperature, fresh-air supply temperature, and area ratio were all fairly linearly related to the indoor air temperature, whereas the relative humidity had a little effect. When building radiant cooling panels with a dedicated fresh-air system, the sensible load equation and condensation model can be utilized as guidance. In their work, Zhao et al. [26] addressed the usage of a regular shape for the heat source, such as a circle, rectangle, or square to calculate heat conduction analytically. On the other hand, the same publication mentioned that research into transient heat conduction has been rather limited. This is because flexible heater designs were not taken into account when it comes to the conventional heaters. The objective was to build a model for transient heat conduction using the separation of variables approach, which will then be utilized to verify the finite element analysis. By choosing the shape of the serpentine heat source, they were able to achieve the temperature uniformity of their model under a variety of scenarios. In their reconstruction of radiant cooling panels, Xing and Li [27] performed a comparison using liquid cooling panels. On the basis of numerical calculations, the effects of the panel's dimensions, flow channels, and materials on the thermal and hydraulic performance of the new radiant cooling panels were carefully evaluated. The rebuilt radiant cooling panels performed thermally better than the traditional pipe-panel radiant cooling panel.

1.4 The current aims

Another important attention was paid to the heat sources, especially at motion, such as those used in continuous casting, surface hardening, and welding processes. When there are several passages, the heat may be intermittent.

The analysis of heat conduction in a medium that was being heated by a moving heat source was the subject of the Kim's study [28]. He assessed the temperature distribution surrounding a rectangular-shaped source traveling steadily along a bar's axis. Using Fourier series assumptions, the transient temperature field from a moving heat source was examined. The outcome of the heat source's passage demonstrated that the temperature increase brought on at a certain location close to the source tends to stabilize. In the analysis of Eremin et al. [29], the issue for a multilayer construction was reduced to a single layer with discontinuous (piecewise-continuous) medium using the asymmetric unit

function (Heaviside function). The nonlinear differential equation (nonlinearity of the second kind and the thermalphysical properties depend on the spatial variable) was reduced to a linear one by adding a new independent variable, and its direct integration enabled obtaining an accurate analytical solution to the problem under consideration.

Therefore, in an era marked by rapid technological advancements and increasing demands for passive solutions, this research sets a vital foundation for further investigations into radiant heating and cooling from a mathematical perspective. Previous studies have overlooked the unsteady heating and cooling loads, revealing a significant gap in our understanding. It is crucial to recognize that hot or cold coolant can originate from various sources that do not necessarily maintain a constant power output. Additionally, this research emphasizes the importance of designing systems that can effectively handle large areas. There is an urgent need for a comprehensive equation that consolidates all potential variables, as it would greatly facilitate numerical simulations and experimental designs. Supporting this initiative will not only enhance our theoretical framework but also pave the way for practical applications in the field.

The following mathematical derivations aim to produce temperature distribution formula by assuming piecewise function to the total heat transfer of the panel. Then, computer simulations are run for validation and more performance evaluation. Note that while the Heaviside step function assumption is original, the concept of treating the heat source term in separate variables is not; see for example [26].

Further, when Heaviside step function exists, a new formation of Laplace Transform will be introduced for this type of input in this area of research.

2. MATHEMATICAL ANALYSIS

2.1 Geometry specifications

It is assumed that the flow inside the inserted tube is incompressible, and the physical properties of the solid box and fluid remain unchanged by temperature. The mathematical derivations will be entirely for the solid slab represented by a linear partial differential equation. The flow inside the tube is maintained at high Reynolds number while it absorbs /transmits (with focusing on absorption here) its energy to the adjacent layers. In Figure 1, the geometry is visualized as a rectangular panel resembling that of conventional radiant wall serving in many applications. The materials are chosen copper for both the box and tube. The water coming from the upper inlet terminal is at a controlled temperature while others will be calculated accordingly (bottom and average surface temperature).

The box is $W \times H \times \delta$, where the thickness (δ) is along the z-axis. The tube with diameter (d) embedded inside the box is serpentine in shape with multiple turns (N_s). The Reynolds number $(Re) = umaxd\ /\ \mu$ is based on the maximum pipe's velocity. The Prandtl number (Pr) is taken 6.9 for water at 25°C. The three important parameters (a, c, and Ls) represent the inner distances of rounded tube, and their equations are shown in Table 1, where R is the tube radius. The control volume and its boundary conditions that will be used for the panel design are shown in Figure 2. The figure shows a U-turn section of serpentine tube with three views: the solid panel, bent tube, and boundary conditions around the whole control volume. The panel is exposed to heat by one face while others are fully insulated. Since the radiation and natural convection take place along the panel, the suggested model of internal heat will be for the y-direction only. The upper panel temperature or T_{tp} is a linear function in terms of x, where T_{wi} is the water inlet temperature.

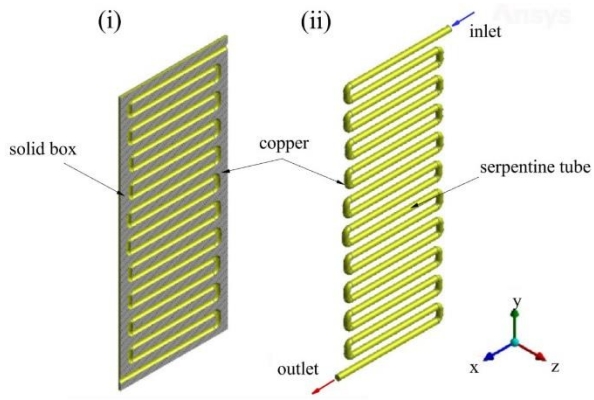

Figure 1. Geometry illustration of the current analysis: (i) the solid box and (ii) the tube

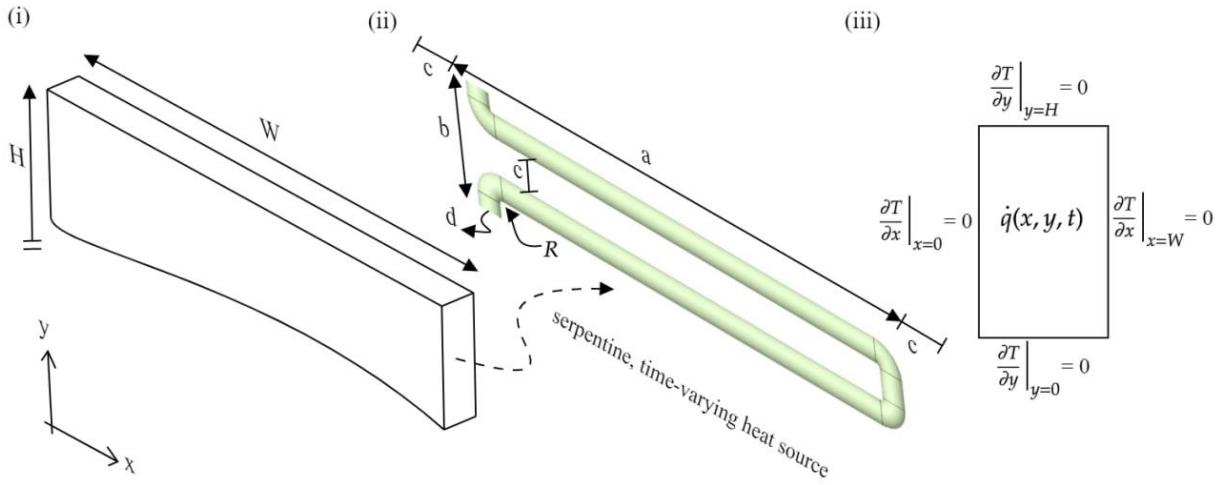

Figure 2. Three sketches for whole domain showing the main dimensions and boundary conditions

Table 1. Geometry specifications of the current analysis

Part	Formula	Value
Panel size	W×H×δ	0.86×1.923×0.045
Serpentine turns	N_s	20
Tube diameter	d	0.04
Vertical distance	$c = \frac{H-(N_s+1)d}{N_s+2}$	0.049
Axial distance	a=W-(2c-2d)	0.68
Variable y	$y = H - (y + nc + nR)$	0.68
Whole length of serpentine tube	$L_s = (N_s + 1)a + cN_s + \pi RN_s$	16.55

2.2 Cooling load assumption

Air conditioning systems should be able to manage interruption and/or multiple indoor settings due to varied demands during the day. Since the unit step function is a mathematical tool for representing abrupt changes in the variables of any circuit, it can simulate the on/off action of such systems. These assumptions can be noticed in some previous studies like Rahbari et al. [30], where step function heat pulse, which was used to imitate heat conduction in a one-dimensional slab, was formed up of Heaviside function. Based on the proposed design of the current radiant panel, the heat load is estimated to be on range of 300 to 500 watts with these changes in the water inlet velocity, temperature, and diameter as follows:

$$\dot{q}(y,t) = \frac{\dot{q}}{A_s u A} q_1(y) q_2(t) \tag{1}$$

where, A_s is the total heat transfer area of the tube, and u is the water velocity used due to $q_1(y)$. In Eq. (1), the symbol A is a factor in m^{-1} for temporal variation, or 2π/R, based on the assumption of $q_2(t)$. The fully-developed velocity (u) of water at the inlet is

$$u = \frac{G}{4\rho v}(R^2 - r^2) \tag{2}$$

where, $G = 4u_{max}\rho v / R^2$ is the pressure drop factor of Poiseuille flow in Eq. (2). At the air flow side, in most cases where the air velocity is small like 0.2 m/s or where the difference between the MRT and air temperature is small such as 4°C, the operative temperature can be averaged with sufficient approximation to the MRT as presented next [31]. As presented by Uponor [32], if a cubic meter room is considered, and the air temperature, T_a, is at 24.93°C, the area of each side will be multiplied by its mean temperature, and the sum will be divided by the total areas and value MRT = 23.87. Thus, for the air side, the operative temperature T_{av} is (T_a+MRT)/2 = 24.4°C. The fin effectiveness of radiant panel can be expressed by means of the panel heat removal factor (HR), which is the ratio between the actual absorbed heats to that removed if the entire panel was at the inlet fluid temperature. It can be written as [7].

$$HR = \frac{T_{av} - T_p}{T_{av} - T_{wi}} \tag{3}$$

where, the design challenge is to determine the panel average temperature T_p for a given mass flow rate and geometry specifications.

2.3 Separation of variables

In this article, the separation of variables method will be used for the heat conduction equation, adopting the earlier work of Abdulrasool et al. [33]. The partial differential equation for the solid box is non-homogeneous and linear, so superposition assumptions will be used for homogeneity. This governing equation for the panel is represented by the transient, source, and diffusion terms as follows:

$$\frac{1}{\alpha}\frac{\partial T}{\partial t} = \frac{\partial^2 T}{\partial^2 x} + \frac{\partial^2 T}{\partial^2 y} + \frac{\partial^2 T}{\partial^2 z} + \frac{\dot{q}}{k} \tag{4}$$

And the applied boundary conditions as shown in Figure 3.

$$\left.\frac{\partial T}{\partial x}\right|_{x=0} = 0, \left.\frac{\partial T}{\partial x}\right|_{x=0} = 0, \left.\frac{\partial T}{\partial x}\right|_{x=0} = 0, \text{and } T_{y=H} = T_{tp},$$

as in the study conducted by Radzai et al. [15], where a constant heat flux is only used on one side of the plate (i.e. temperature linear behavior). This study suggests two cases which are performed for the source term: the steady case where the differential equation turns into

$$\frac{\partial^2 T}{\partial^2 x} + \frac{\partial^2 T}{\partial^2 y} + \frac{\dot{q}(y)}{K} = 0 \tag{5}$$

The theory of superposition yields two parts as shown in Figure 3.

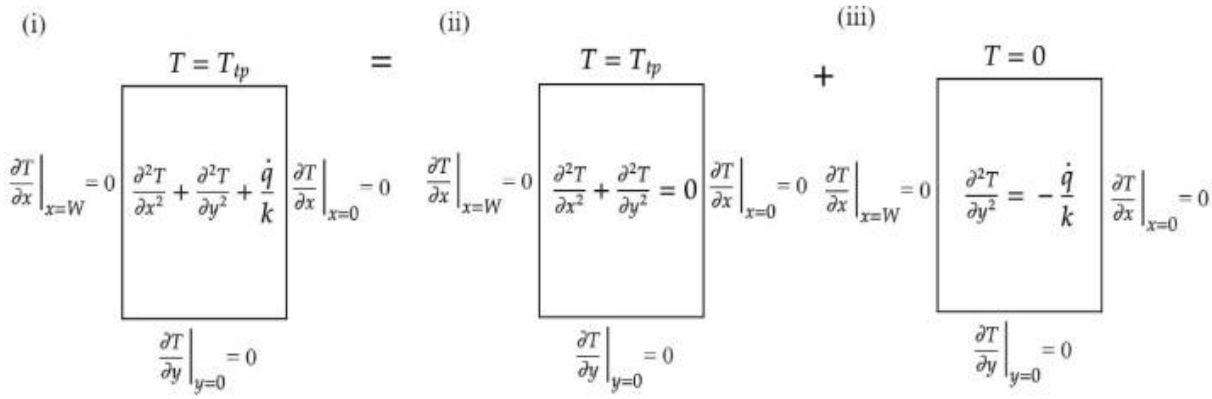

Figure 3. Superposition technique for the differential equation with variable heat sink

$$T(x,y) = T_1(x,y) + T_2(y) \tag{6}$$

where, the first term is for temperature variations in two-dimensional space while the second one is for the external effect such as heat sink. Thus, the initial guess solution can be

$$T_1(x,y) = X(x)Y(y) \tag{7}$$

If Fourier series, an infinite sum of periodic functions, is implemented in one dimension as follows

$$x'' + \lambda^2 x = 0 \tag{8}$$

The solution is

$$(x) = A_1 cos(\lambda x) + A_2 sin(\lambda x) \tag{9}$$

where, two constants A_1 and A_2 appear in the solution. From the boundary conditions, A_2 is zero, and the Eigenvalues are $\lambda = n\pi/W$, where n = 0, 1, 2, 3… etc. Based on previous explanations, the equation for y-axis becomes

$$Y'' - \lambda 2y = 0 \tag{10}$$

And the solution is

$$Y(y) = A_3 cosh(\lambda y) + A_4 sinh(\lambda y) \tag{11}$$

where, the A_4 also vanishes due to the boundary condition at the panel's bottom. From Eq. (7), the steady temperature at any position is given by

$$T_1(x,y) = A_o + \sum_{n=0}^{\infty} A_n \, cos(\lambda x) + cosh(\lambda y) \tag{12}$$

The remaining solution part of Eq. (6) will be obtained from

$$\frac{\partial^2 T}{\partial y^2} = \frac{-\dot{q} q_1(y)}{K} \tag{13}$$

where, the Heaviside function is the prescribed function in the y-direction since the pipe divisions lead to separate heat transfer regions. The equation involving all of the relevant geometry parameters is shown below:

$$q_1(y) = \sum_{n=0}^{N} (R^2 - y_n^2)[-\theta\left(y_n - \frac{c}{2}\right) - \theta\left(y_n - \left(\frac{c}{2} + d\right)\right) + \theta(y_n - (\frac{3c}{2} + d)) - +\theta(y_n - (\frac{3c}{2} + d))] \tag{14}$$

where, θ denotes to the Heaviside function. After substituting Eq. (13) into Eq. (14) and performing double integrals, the result is

$$T_2(y) = \frac{-\dot{q}}{K} \int q_1(y) dy + A_5 y + A_6 \tag{15}$$

To evaluate the constants, boundary conditions are imposed to give that A_5= 0, and

$$A_6 = \frac{\dot{q}}{k} \int q_1(y) dy|_{y=H} \tag{16}$$

The final form of temperature distribution equation in this case is

$$T(x,y) = A_0 + \sum_{n=1}^{\infty} A_n \, cos(\lambda x) \, cosh(\lambda x) + \frac{\dot{q}}{k} (\int q_1(y) dy|_{y=H} - q_1(y) dy) \tag{17}$$

where,

$$A_0 = \frac{1}{W} \int_0^W T_{tp} dx \tag{18}$$

$$A_n = \frac{2}{cosh(\lambda H) W} \int_0^W T_{tp} cos\,(\lambda x) dx \tag{19}$$

It is believed that the discontinuity comes also from the system operating with time. That is expressed as follows

$$\frac{1}{\alpha} \frac{\partial T^*}{\partial t} = \frac{\partial^2 T^*}{\partial x^2} + \frac{\partial^2 T^*}{\partial y^2} + \frac{\dot{q}}{K} \tag{20}$$

In this case, the notation will be T^* for unsteady temperature. The superposition theory can be applied again such as

$$T^*(x,y,t) = T_1^*(x,y) + T_2^*(y,t) \tag{21}$$

where, the first term (T_1^*) is for the steady part, whose solution was derived previously. The second part will be analyzed next. The differential equation for this part becomes

$$\frac{\partial^2 T_2^*}{\partial y^2} - \frac{1}{\alpha} \frac{\partial T_2^*}{\partial t} = \frac{-\dot{q} q_1(y) q_2(t)}{k} \tag{22}$$

In this situation, the assumption is changed to

$$T^*(y,t) = Y(y) \Gamma(t) \tag{23}$$

Fourier solution is utilized in y-axis and gives

$$Y(y) = c_1 \, cos(\mu y) + c_2 \, sin(\mu y) \tag{24}$$

and from the boundary conditions, c_2 = 0, and $\mu = k\pi/2H$, where k = 1, 3, 5, ... etc. After substituting the derivatives of the above function into Eq. (22), we obtain

$$cos(\mu y) \left[\frac{1}{\alpha} \dot{\Gamma}_k(t) + \mu^2 \Gamma_k(t)\right] = \frac{-\dot{q} q_1(y) q_2(t)}{k} \tag{25}$$

The two sides of Eq. (25) will be multiplied by $cos(\mu y)$ and be integrated to $y = H$. So that, the Fourier coefficient can be evaluated via

$$[\dot{\Gamma}_k(t) + \mu^2 \Gamma_k(t)] = \frac{2\dot{q}\alpha}{KH} q_2(t) \int_0^H q_1(y) \, cos(\mu y) \, dy \tag{26}$$

If a constant such as

$$f_k = \frac{2\dot{q}\alpha}{KH} \int_0^H q_1(y) \, cos(\mu y) \, dy \tag{27}$$

Then, a time-dependent ordinary differential equation is constructed as follows

$$\dot{\Gamma}_k(t) + \mu^2\alpha\Gamma_k(t) = f_k q_2(t) \tag{28}$$

The time-varying function, $q_2(t)$, is assumed herein as a piecewise-defined function with three intervals or

$$q_2(t) = \begin{cases} 2 & \pi < t < 2\pi \\ 2\,cos(4t) & 2\pi < t < 3\pi \\ t^2 & t > 3\pi \end{cases} \tag{29}$$

where, the first two types (wavy and constant) are comparable to those reported by Ghasemi and Aminossadati [34], while the third example serves as a test. Then the in-line function for $q_2(t)$ can be written as

$$q_2(t) = 2 + (2\,cos(4t) - 2)\theta(t - 2\pi) + (t^2 - 2\,cos(4t))\theta(t - 3\pi) \tag{30}$$

This can be substituted into Eq. (28) leading to

$$\dot{\Gamma}_k(t) + \mu^2\alpha\Gamma_k(t) = f_k(y(2 + (2\,cos(4t) - 2)\theta(t - 2\pi) + (t^2 - 2\,cos(4t))\theta(t - 3\pi)) \tag{31}$$

Before using Laplace Transform to the Eq. (31), a new Laplace formation will be introduced first as follows:

$$\mathcal{L}\left(t^i\theta(t-g)\right) = F(s)e^{-gs}\sum_{K=0}^{i}\frac{(gs)^i}{i!} \tag{32}$$

Now, executing this new and other equations of integral transform to each term of Eq. (31) yields to

$$s\Gamma_k(s) - T_2^*(y,0) + \mu^2\alpha\Gamma_k(s) = f_k\left(\frac{2}{s} + \frac{\begin{matrix}-32e^{-2s\pi}s^2 \\ +e^{-3s\pi}\left(9\pi^2s^4 + 144\pi^2s^2 + 6\pi s^3\right) \\ -2s^4 + 96s\pi + 2s^2 + 32\end{matrix}}{s^3(s^2+16)}\right) \tag{33}$$

All terms are transferred to s-parameter in this new algebraic equation. After that, Inverse Laplace Transform will be implemented for all terms to reach that

$$\Gamma_k(t) = f_k\mathcal{L}^{-1}[\frac{2}{s(s+\mu^2\alpha)} + \frac{32e^{-2s\pi}s^2+e^{-3s\pi}(9\pi^2s^4+144\pi^2s^2+6\pi s^3-2s^4+96s\pi+2s^2+32)}{s^3(s^2+16)(s+\mu^2\alpha)} + \frac{\frac{T_2(y,0)}{f_k}}{(s+\mu^2\alpha)}] \tag{34}$$

For simplicity, after obtaining the outputs of Eq. (34), the solution of Eq. (31) will be divided into sub-divisions from P_1 to P_4 as follows:

$$\begin{aligned} P_1 = {} & 16 + \mu^2\alpha^2 + 16\big(-2\big(cos^2(t)\big) \\ & + 1\big)\,cos(t)\,sin(t)\,\mu^6\alpha^3 \\ & + e^{-\mu^2\alpha(t-3\pi)}(\mu^8\alpha^4 - \mu^4\alpha^2 \\ & - 16) + (-8(cos^4(t) \\ & + 8\big(cos^2(t)\big) - 1)\mu^8\alpha^4 \end{aligned} \tag{35}$$

$$\begin{aligned} P_2 = {} & 16\mu^4\alpha^2(-2 + 2e^{-\mu^2\alpha(t-2\pi)} \\ & + 2\mu^2\alpha\,sin(t)\,cos(t)\big(2\big(cos^2(t)\big) \\ & - 1\big) + \mu^4\alpha^2(cos^2(t))(cos^2(t) \\ & - 1))\theta(t - 2\pi) \end{aligned} \tag{36}$$

$$p_3 = \frac{2\theta(t-3\pi)(-3\pi e^{-\mu^2\alpha(t-3\pi)} + t)}{\mu^4\alpha^2} \tag{37}$$

$$P_4 = \frac{\begin{matrix}2 + \left(\frac{T_{s2}(y,0)}{f_k}\mu^2\alpha - 2\right)e^{-\mu^2\alpha t} \\ +\theta(t-3\pi)(-9\pi^2e^{-\mu^2\alpha(t-3\pi)} + t^2\end{matrix}}{\mu^2\alpha} \tag{38}$$

And the full equations will be

$$\Gamma_k(t) = f_k(y)[\frac{2P_1\theta(t-3\pi) + P_2}{(\mu^4\alpha^2+16)\mu^6\alpha^3} - P_3 + P_4] \tag{39}$$

Thus, the complete solution of Eq. (22) is

$$T_2^*(y,t) = \sum_{k=1}^{\infty} f_k\,cos(\mu y)\,[\frac{2P_1\theta(t-3\pi) + P_2}{(\mu^4\alpha^2+16)\mu^6\alpha^3} - P_3 + P_4] \tag{40}$$

$$T^*(x,y,0) = T(x,y) - T_2^*(y,0) = \frac{\dot{q}}{k}(\int q_1(y)dy|_{y=H} - \int q_1(y)dy) \tag{41}$$

And the final solution of unsteady Eq. (20) is

$$T^*(x,y,t) = A_0 + \sum_{n=1}^{\infty} A_n\,cos(\lambda x)\,cosh(\lambda y) + \sum_{k=1}^{\infty} f_k\,cos(\mu y)[\frac{2P_1\theta(t-3\pi) + P_2}{(\mu^4\alpha^2+16)\mu^6\alpha^3} - P_3 + P_4] \tag{42}$$

3. DATA VALIDATION

One drawn result from Eq. (42) will be compared to its similar data by Koca et al. [6] for validation purpose. The experiment took place in a full-scale room mimicking modern building characteristics. It followed ASHRAE standards for thermophysical parameters and experimental setup. Measurements focused on the inlet and outlet water temperatures during steady-state conditions. The hydraulic system enabled heat flow through the cooling system under these conditions, with conditioning panels and surface temperatures serving as steady-state indicators. However, these conditions may not apply universally, as fluctuations could affect the cooling process. Results were based on average values calculated over 30-minute intervals of stability. A formulation for the cooled radiant wall was proposed but found to be overestimated by about 3.2% compared to standard values.

Figure 4 is to demonstrate the similarity and dependability of our derived model compared to Koca's experiment [22], where six temperature data consisting of the water inlet and average surface temperature for the wall panel were borrowed from Koca [22].

In fact, this experiment was chosen over others of RCP for the following reasons: First, all of its geometric parameters and boundary conditions are comparable to those of the current investigation. Second, there is little research on cooled radiant wall systems–just one study has been published in the literature.

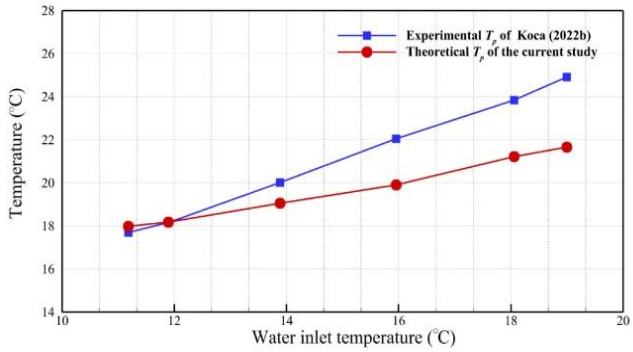

Figure 4. Panel surface temperature vs. water inlet temperature data obtained from current derived solution Eq. (42) and experimental from Yu et al. [22]

In fact, this experiment was chosen over others of RCP for the following reasons: First, all of its geometric parameters and boundary conditions are comparable to those of the current investigation. Second, there is little research on cooled radiant wall systems–just one study has been published in the literature. Both behaviors show the average panel temperature increases as the input water warms up. However, the discrepancies between data and trends of the two approaches are obvious. Despite that there are common experimental uncertainties and empirical formations encountered in the Koca data [22], the most possible cause for this data gap is the distribution of panels. This can be explained by the divisions of system in Koca's experiment into seven panels [22], each containing three bent tubes whereas our model represents one panel with one embedded tube. In the event that everything is exactly analogous to that experiment, we think our model can still predict meaningful readings very close to the realistic data. However, the current theoretical and experimental results have a Mean Absolute Error (MAE) of 1.54916, which is calculated according $MAE = \frac{\sum_{i=1}^{n}|y_i - x_i|}{n}$ where y_i = the current prediction, x_i = the experimental value and n = total number of data points.

In addition, numerical simulations were performed for selected data and operation conditions. This was achieved by using Ansys 2022 R1 workbench that includes Design Modeler, Meshing, and Fluent. The solid enclosure and the liquid contained within the ten-turn serpentine tube represent distinct computing domains within the experimental setup. To effectively replicate the experiment and affirm the theoretical derivation, the entire geometry is positioned in a vertical orientation. The upper end of the tube serves as the inlet, whereas the lower end functions as the outlet. Heat is applied uniformly to one side of the box and varies with time, while the opposite side maintains a constant temperature. The alterations in the flow regime, which have the potential to influence the outcomes of the experiment, are governed by the input velocity of the fluid in the tube. Our computations integrate the effect of gravitational force acting in the vertical direction, consistent with the theoretical derivation.

The geometry sizes are the same those in Table 1 with two bodies being built for the solid box and fluid. The mesh was then constructed with option of Tetrahedrons Method. The number of cells was tested at 4325706, 1919101, 1884469, and 1758594 for both zones together. The denser mesh reads minimum orthogonal quality of 0.5 and maximum mesh aspect ratio of 10. The boundary conditions were assigned as following: Velocity-inlet, temperature-inlet, outflow, and mixed heat flux. These are distributed for the inlet, outlet, and the inner wall face in x and y directions, in front of the conditioned room. The results of each simulation for different meshes were acquired and compared with each other. The maximum dissimilarity between the panel bottom temperatures were found to be small enough, around 0.05% for the three intense meshes, so the mesh with 1919101 cells was chosen for the rest of the analysis. Figure 5 shows an example of numerical validations for the analytical solutions presented in this study at a constant heat load of 364 watts. The temperatures were recorded at different flow rates and found to lessen gradually. The explanation of this decrease is obvious since the heat load was fixed at one value. That means high water velocity causes less temperature span between the panel top and bottom temperatures. The average temperature of the panel surface, T_p, is higher than the bottom temperature, T_{bp}, due to the cooling process by the wall.

The highest discrepancy of data produced by the two approaches was between 2.5 and 5% at different flow rates, with around 0.6 MAE. The assumption of heat sink made in the analytical study or the turbulent models of ANSYS package may be responsible for the shown gap between the solutions of the two solvers. Readers should be aware that the theoretical derivation only deals with the energy equation of the panel experiencing the heat load that is modified, not the Navier-Stokes equations. Two approaches were between 2.5 and 5% at different flow rates. The assumption of heat sink made in the analytical study or the turbulent models of ANSYS package may be responsible for the shown gap between the solutions of the two solvers. Readers should be aware that the theoretical derivation only deals with the energy equation of the panel experiencing the heat load that is modified, not the Navier-Stokes equations. To highlight the underlying physical interpretation, these assumptions suggest that the heat drawn from the fluid acts as a heat source within the theoretical framework. Additionally, the variability introduced to this heat source originates from the flow fluctuations. In mathematical terms, this heat source is depicted as a piecewise function, reflecting its proximity to real-world applications in this domain. However, it is crucial to scrutinize the validity of these assumptions in greater detail and to compare them with alternative mathematical models to enhance their general applicability.

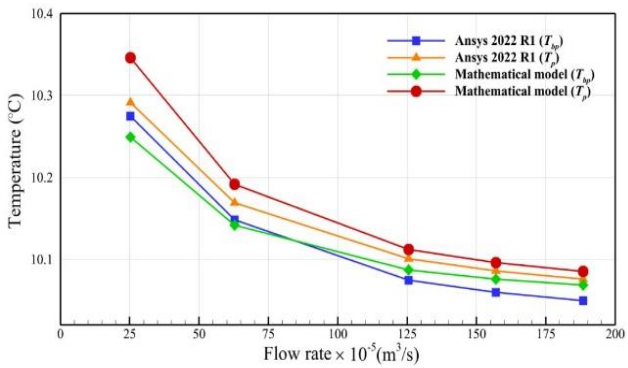

Figure 5. Bottom and average panel temperatures vs. flow rate data obtained from the current solution of Eq. (42) and those of Ansys

4. RESULTS

4.1 Theoretical data

The following results, which illustrate this control concept of each radiant cooling panel's parameter, are presented in a manner similar to those of Uponor [32]. The outputs of Eq. (42) are the panel average surface temperature, T_p, and bottom panel temperature, T_{bp}. Other parameters such as flow rate, water inlet temperature, and cooling load are controlled. Figure 6 exhibits the profiles of T_p and T_{bp} at multiple cooling loads with constant flow rate and water inlet temperature.

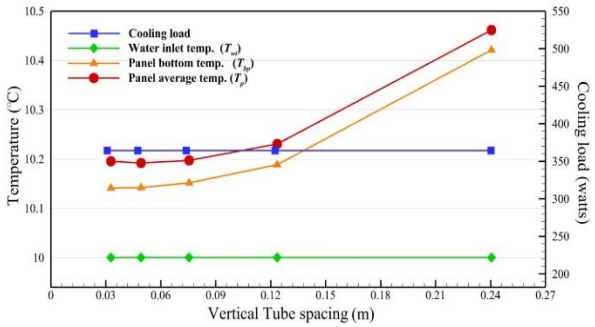

Figure 6. Analytical temperature solutions of Eq. (42) at constant flow rate, constant water inlet temperature, and variable heat loads

When the flow rate is fixed, the cooling load causes the temperature differential between the water's inlet and outflow to increase about 434.9%, which raises the bottom temperature of panel. The average temperature of the panel is obviously higher than the bottom temperature as the cooling load grows. It is well known that the system works best when the panel is sufficiently close to the water inlet temperature. This demonstrates that the panel cooling role weakens with increasing cooling loads (700% in this case) if either the water inlet temperature or the water flow velocity is held constant. So that, to improve performance, the supplied water's flow conditions or properties must be altered.

When the water input temperature was changed to meet the needs of the cooling load, the temperature difference between T_{wi} and T_{bp} deviated noticeably to higher values. These behaviors are magnified within a box in Figure 7 which is also drawn at a constant flow rate but variable T_{wi} and loads. To clarify, this temperature difference was 0.08 at 178.7 watts while it raised to 0.14 at 364.4 watts, i.e., 75% increase in the temperature span if 103.9% change happens to the loads.

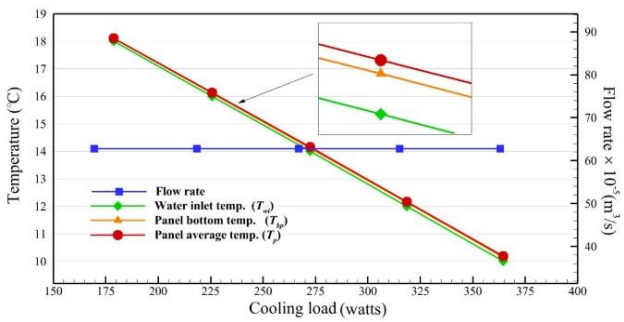

Figure 7. Analytical temperature solutions of Eq. (42) at constant flow rate, variable water inlet temperatures and cooling loads

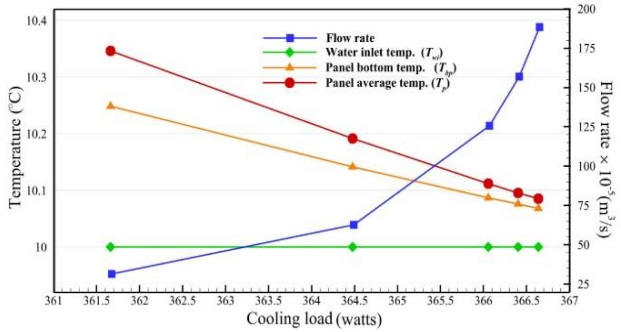

Figure 8. Analytical temperature solutions of Eq. (42) at variable flow rates, constant water inlet temperature, and variable cooling loads

From the perspective of cooling cycle design, it can decrease the water inlet temperature T_{wi} to satisfy the set-point temperature requirements. However, there is still an issue with the dew point temperature of interior air, which, if T_{wi} is too low, results in condensation on the radiant wall surface. The fluid flow rate in Figure 8 differs from 0.0003139 to 0.001883 m^3/s, and along with the flow rate, the plate temperatures drop. As the cooling demand rises, the difference between T_{wi} and T_{bp} narrows (76.7%), despite the fact that there is just a small variation in the load–361.66 to 366.64 watts (1.4%)–compared to the prior tests. It is therefore possible to whether adjust the water inlet temperature or flow rate to meet the demands of the cooling load. Previous calculations demonstrated that the cooling loads vary more slowly as water flow rate increases than as water inlet temperature decreases. On the other hand, a high flow rate promotes more pumping power to the serpentine tube, while a low water inlet temperature maximizes the need to high cooling capacity of the chiller, although it also requires marginally high flow rate.

The design factors of radiant cooling panel are the panel size and the total, effective heat transfer area. Using Eq. (42), the aspect ratio of W/H can be modified to obtain the best performance. In Figure 9, at a fixed cooling load, 364.47 watts, and water inlet temperature, the temperatures of T_p and T_{bp} were calculated with some panel's aspect ratios, W/H. The temperature difference between T_{wi} and T_{bp} narrows from 0.71 to 0.12 (about 83%) as the aspect ratio changes from 0.11 to 0.56 (or 410%). It is anticipated to reach a constant temperature gap when the aspect ratio reaches one as an optimal design, see Mosa et al. [24]. It can be seen that the improvement in the device's width affects the heat transfer significantly due to the enlargement in the heat transfer area.

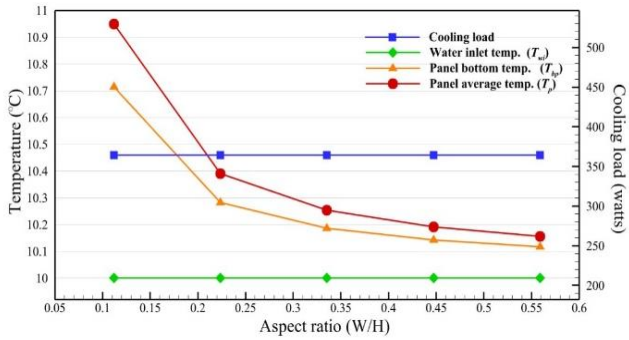

Figure 9. Temperature vs. aspect ratio of the solid box by Eq. (42) at variable flow rates, constant inlet temperature and cooling load

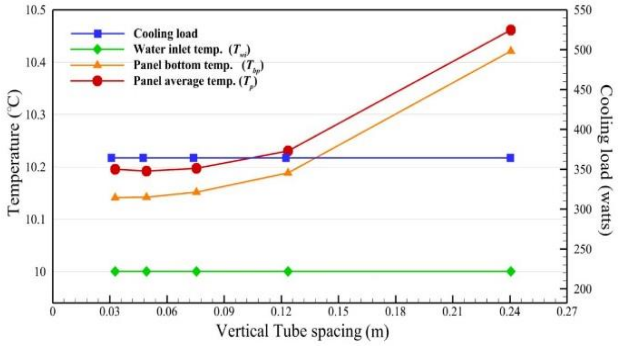

Figure 10. Temperature vs. vertical tube spacing by Eq. (42) at variable flow rates, constant inlet temperature and cooling load

The space between the multiple turns of serpentine tube was changed to some values. Figure 10 presents the relationship of T_p and T_{bp} with this vertical tube spacing, or c, at constant T_{wi}.

At some cooling loads, the several pipe turns are the better, since the heat sink will be increased as the heat transfer area becomes larger. In fact, as the tube spacing rises from 0.031 to 0.24 (about 674%), the temperature differential between T_{wi} and T_{bp} increases from 0.14 to 0.42 (200%), greatly enhancing the heat transfer. Therefore, performance will be better with higher flow rate when c is small. In addition, for Figure 11, the temperature of Eq. (42) is evaluated at different tube diameters. As the tube diameter increases, the temperature of the device lowers since the flow rate will be higher. The values showed temperature differences between T_{wi} and T_{bp} from 0.37 to 0.11 (about 70%) if d is changed from 0.01 to 0.06 m (500%).

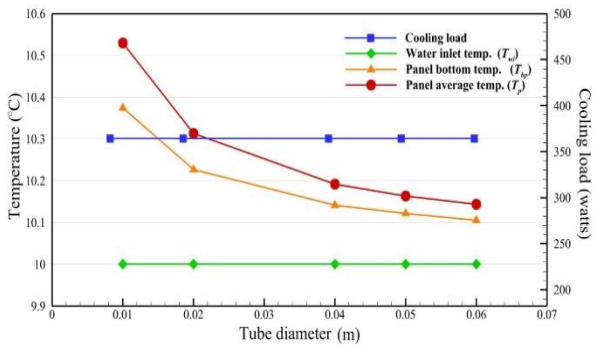

Figure 11. Temperature vs. tube diameter by Eq. (42) at variable flow rates, constant inlet temperature and cooling load

Finally, it is known that this type of system is steady during its operation excluding the initial transient period. However, there are some possible on/off times this system experiences. In Figure 12(i), the data of Eq. (29) is plotted with respect to time to illustrate the fluctuations of heat amplitude. According to the imposed heat, the bottom panel temperature changes with time for two consecutive periods as in Figure 12(ii). This is an example of how the system works under some external impacts. However, the transient function in Eq. (29) can be modified with complying to the real-life application, so the panel duty can be controlled to fulfill the target space needs and obtain ultimately the best performance. In this regard, the Eq. (42) was developed for that purpose with any desired size and optimized goals. In Figure 13, the panel size of W and H as presented in Table 1 was used. The figure shows the temperature distribution with x = 0 and y = H on the water inlet side and with x = W and y = 0 on the outflow side. Note that there is a temperature fluctuation at the top which differs more clearly than that at the bottom. That is because a spatially changing function is implemented on the panel top boundary to incorporate that of water, or T_{wi}. The maximum temperature is about 10.14℃ as shown in Figure 13(i), and the panel heat removal factor (HR) is about 0.986. However, when the device's height and thus the number of pipe turns are doubled, the maximum temperature reaches roughly 14℃, and HR = 0.838 (15% decrease). Figure 13(ii) shows the results of 2H, which means the panel becomes warmer as it takes more energy from long multiple-passages tube leading to less HR. The flow rate does not have to be accelerated, but the energy will be increased due to the large temperature span between the water inlet and outlet. On the other side, when the width of the panel is doubled, the panel cools down to lower temperatures as seen in Figure 13(iii), and HR= 0.992 (0.6% increase). The cooler the panel will be, the higher the thermal performance is achieved; however, at this point, the water flow rate must be high given that the heat exchanger width (a) becomes wider.

If the whole panel is increased in size, the fluid flow rate can be supplied with affordable pressure drop, and the panel's temperature will be lowered to desired values. In Figure 13(iv), both W and H are increased two times, and the highest temperature appears to be 11.8℃ with HR = 0.847 (14% decrease). At this stage, the thermal energy being removed causes a high, and the water flow rate needs not to be very high. As a result, the heat removal factor in the latter situation is not particularly large. Finally, the time-dependent flow in the tube can affect the panel in some ways. First, when the system is on, and there are some interruptions, the temperature fluctuates.

Figure 13(v) shows the temperature profiles over time when the heat sink of the tube is represented as in Eq. (29). The panel's temperature experiences these changes as piece-wise function as implemented. This has to be controlled with set point temperature to gain the desired space conditions with possibly the lowest cost. When starting the system from the rest, the panel's temperature varies over the entire panel reaching the specified temperature. An example of these changes with time is illustrated in Figure 13(vi), but more analyses can be done to produce more results taking advantage from Eq. (42).

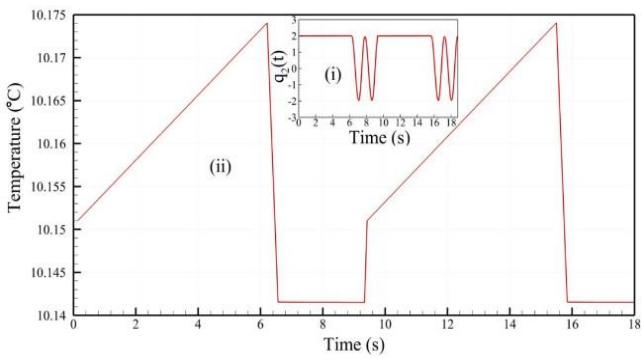

Figure 12. Temporal variations by Eq. (42) of (i) convective heat amount (ii) temperature of the solid box for discontinuous signals

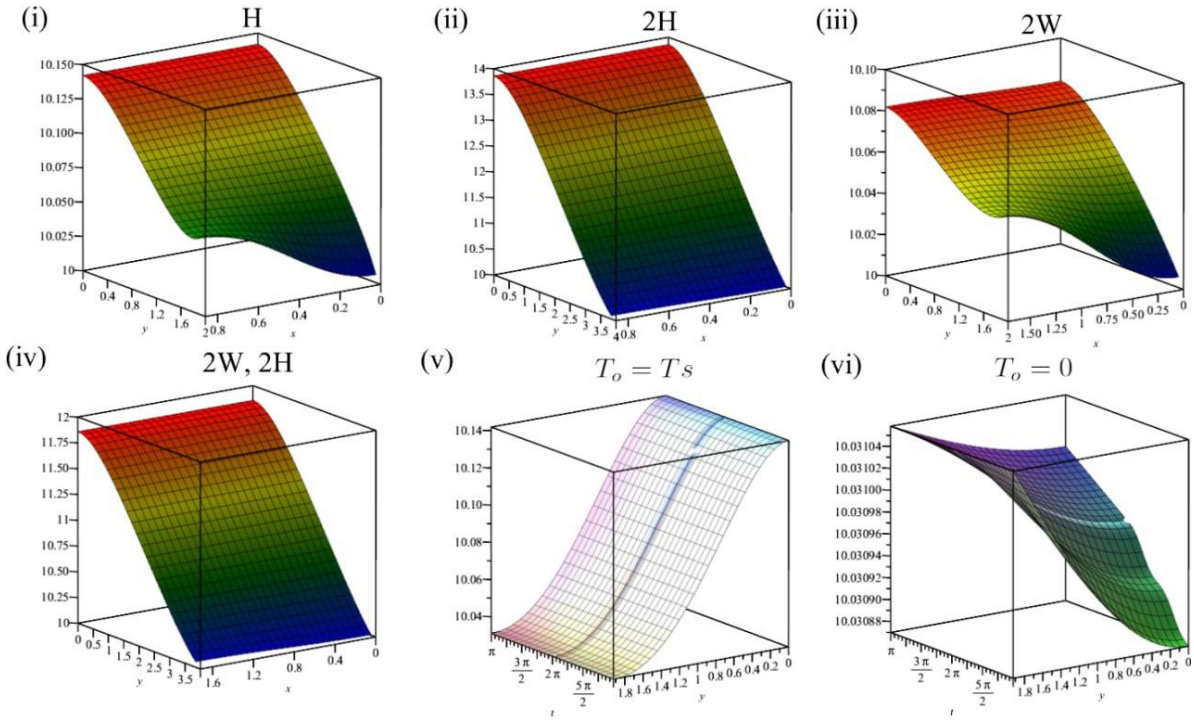

Figure 13. Contours of panel's temperature by Eq. (42) at six different cases with fixed inlet temperature, varying flow rate and cooling load

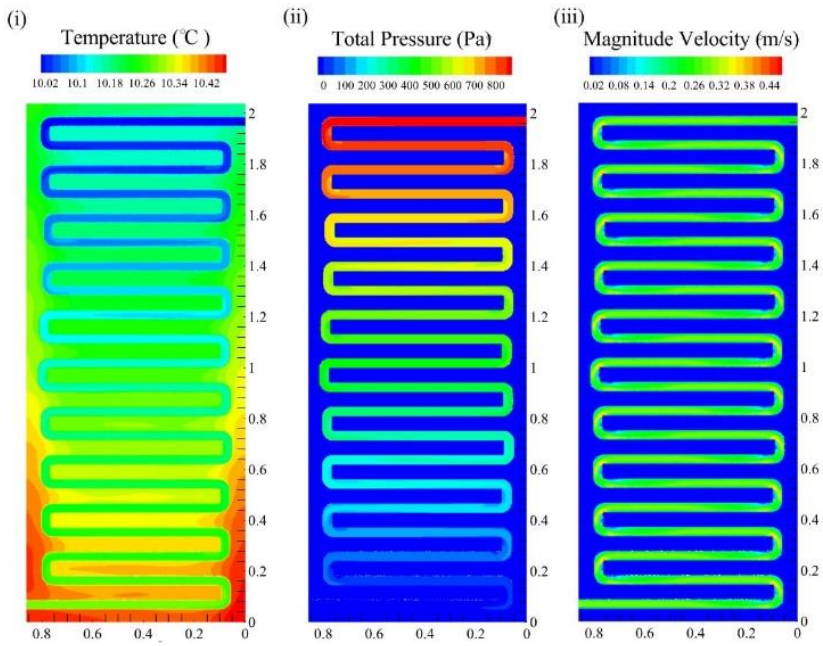

Figure 14. Numerical temperature (i), pressure (ii), and velocity (iii) contours at 31.4×10^{-5} m^3/s in the middle of whole domain

4.2 Simulation data

All simulations were performed in three dimensions after securing the most sufficient mesh, very low residuals, suitable time step, and an adequate number of iterations for steady case. All contours, which are for a variable distribution over the cross-section of longitudinal serpentine pipe, are shown in Figure 14 at *xy*-plane in the mid-section of the solid box. The boundary conditions are: 10°C and 0.25^{-1} m/s at the pipe inlet, outflow at the pipe outlet, 31.4×10^{-5} as water flow rate, and flux = 0 at all other surfaces except that facing the target space.

Figure 14(i) displays the temperature contour with some thermal gradients, especially across the *y*-axis. These changes are due to serpentine shape which might look different if other configurations are used. The water enters cold at the upper side and leaves hot at the bottom. The pressure inside the pipe is shown in Figure 14(ii). The flow begins at about 750 Pa and leaves at less than 100 Pa. The pressure gradient is more obvious at the *y*-axis than that along the *x*-axis. Finally, the velocity changes along the serpentine pipe are shown in Figure 14(iii). The flow appears to experience some separations and reattachments at the bending zones. This is natural since the flow is supposed to be intermittently or fully turbulent and is exposed to sudden changes. The temperature contours at

different water flow rates of 31.4, 62.8, and 125.6×10^{-5} are presented in Figures 15(i)-(iii) respectively. The temperature gradients of the three figures fade gradually toward the panel's top in *y*-axis. Also, the gradient changes with *x*-axis approximately as predicted by the present analytical model. The panel's temperature lowers as the flow rate increases. This is also expected since flow absorbs heat fast as it goes down in the pipe.

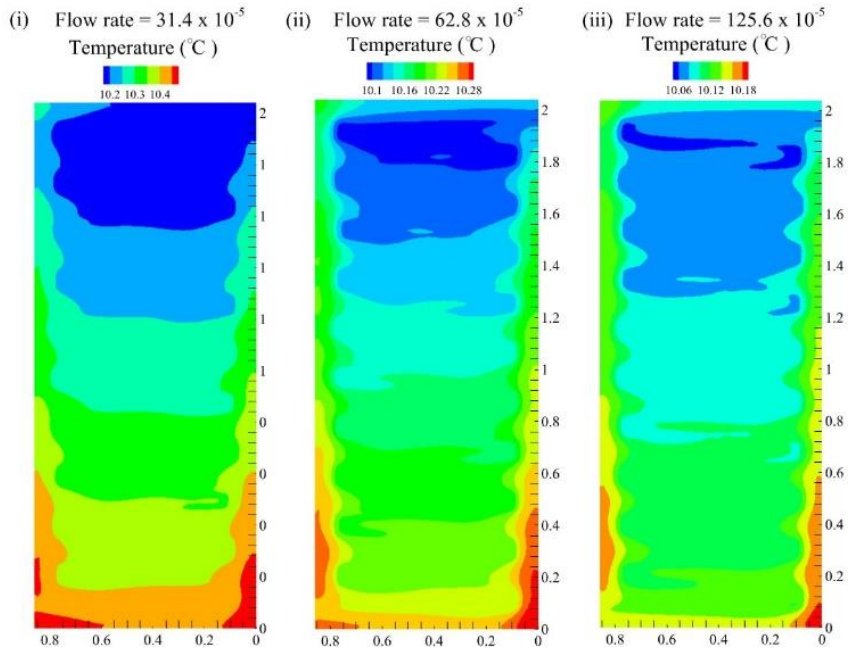

Figure 15. Numerical temperature contours at different fluid flow rate of plane positioned in the front of target space

5. CONCLUSIONS

Radiant cooling panel is increasingly becoming popular among air conditioning systems. However, the condensation issue remains a challenge about this device usually dealing with large heat transfer areas. The significance of this work can be explained as follows: an experiment may not be able to monitor the mean radiant temperature, or MRT, accurately enough, even if thermocouples are evenly spaced across the panel. Numerical schemes may need improvements to reach exact solutions. It is commonly recognized that increasing efficiency in numerical tasks is often achieved by applying analytical solutions to models and algorithms. The radiant panel's dew-point temperature and design are determined by its average surface temperature and spatio-temporal distribution. Herein, the heat sink term in the energy equation was put under the scope with two assumptions for the space and time separately. A new form of Laplace transformation was introduced, and numerical computations were performed thereafter. The followings are the main conclusions:

1. The cooling load can be assumed, calculated, and added as a known input to the panel's heat conduction equation.
2. Using the obtained solution and the water intake and air operative temperatures, it was feasible to determine the bottom and average temperatures of the panel.
3. Due to a 700% increase in cooling load at a given water inlet temperature and flow rate, the temperature span over the panel raised to 434.9%.
4. The temperature spread increased by 75% while the cooling load increased by 103.9% at a fixed water flow rate.
5. Only when the water inlet temperature was fixed, there was a 76.7% decrease in the temperature span at a 1.4% rise in the cooling load.
6. At constant cooling load, the temperature span decreased by 83% while the aspect ratio (W/H) was increased by 410%.
7. At fixed cooling load, 200% increase in the temperature span in front of 674% increase in the vertical tube spacing (c).
8. The temperature span decreased by 70% at a fixed cooling load against an increase in tube diameter (d) of 500%.
9. If the panel width is doubled, the panel heat removal factor (HR) rises to 0.6%. If H is doubled, this component loses 15% of its value. In the event that W and H are both doubled, the proportion falls to 14%.

ACKNOWLEDGMENT

The authors would like to acknowledge the University of Kerbala (UoK) (the Iraqi Ministry of Higher Education and Scientific Research) for providing a financial support during this research.

REFERENCES

[1] American Society of Heating Refrigerating and Air Conditioning Engineers, Ashrae, Owen, M.S. (2016). 2016 ASHRAE Handbook-HVAC Systems and Equipment (SI Edition). ASHRAE. https://books.google.com/books?id=iwCJAQAACAAJ.

[2] Koca, A. (2022). Experimental examination of heat transfer coefficients in hydronic radiant wall cooling systems. Journal of Building Engineering, 60: 105209. https://doi.org/10.1016/j.jobe.2022.105209

[3] Krajčík, M., Arıcı, M., Šikula, O., Šimko, M. (2021).

Review of water-based wall systems: Heating, cooling, and thermal barriers. Energy and Buildings, 253: 111476. https://doi.org/10.1016/j.enbuild.2021.111476

[4] Karakoyun, Y., Acikgoz, O., Yumurtacı, Z., Dalkilic, A.S. (2020). An experimental investigation on heat transfer characteristics arising over an underfloor cooling system exposed to different radiant heating loads through walls. Applied Thermal Engineering, 164: 114517. https://doi.org/10.1016/j.applthermaleng.2019.114517

[5] Krajčík, M., Šikula, O. (2020). The possibilities and limitations of using radiant wall cooling in new and retrofitted existing buildings. Applied Thermal Engineering, 164: 114490. https://doi.org/10.1016/j.applthermaleng.2019.114490

[6] Koca, A., Karakoyun, Y., Acikgoz, O., Dogu, M., Dalkilic, A.S. (2022). An experimental investigation on the radiant cooled wall's heat transfer characteristics in a fully conditioned real-sized living environment. Energy and Buildings, 277: 112578. https://doi.org/10.1016/j.enbuild.2022.112578

[7] Conroy, C.L., Mumma, S.A. (2001). Ceiling radiant cooling panels as a viable distributed parallel sensible cooling technology integrated with dedicated outdoor air systems/discussion. ASHRAE Transactions, 107: 578.

[8] Hassan, M.A., Abdelaziz, O. (2020). Best practices and recent advances in hydronic radiant cooling systems–Part II: Simulation, control, and integration. Energy and Buildings, 224: 110263. https://doi.org/10.1016/j.enbuild.2020.110263

[9] Hu, R., Sun, S., Liang, J., Zhou, Z., Yin, Y. (2023). A review of studies on heat transfer in buildings with radiant cooling systems. Buildings, 13(8): 1994. https://doi.org/10.3390/buildings13081994

[10] Fonseca, N. (2011). Experimental analysis and modeling of hydronic radiant ceiling panels using transient-state analysis. International Journal of Refrigeration, 34(4): 958-967. https://doi.org/10.1016/j.ijrefrig.2011.01.007

[11] Seyam, S., Huzayyin, A., El-Batsh, H., Nada, S. (2014). Experimental and numerical investigation of the radiant panel heating system using scale room model. Energy and Buildings, 82: 130-141. https://doi.org/10.1016/j.enbuild.2014.07.003

[12] Çolak, A.B., Acikgoz, O., Karakoyun, Y., Koca, A., Dalkilic, A.S. (2023). Experimental and numerical investigations on the heat transfer characteristics of a real-sized radiant cooled wall system supported by machine learning. International Journal of Thermal Sciences, 191: 108355. https://10.0.3.248/j.ijthermalsci.2023.108355

[13] Shen, C., Li, X., Yan, S. (2017). Numerical study on energy efficiency and economy of a pipe-embedded glass envelope directly utilizing ground-source water for heating in diverse climates. Energy Conversion and Management, 150: 878-889. https://doi.org/10.1016/j.enconman.2017.04.063

[14] Jiang, T., You, S., Wu, Z., Zhang, H., Wang, Y., Wei, S. (2021). A novel refrigerant-direct radiant cooling system: Numerical simulation-based evaluation. Applied Thermal Engineering, 198: 117442. https://doi.org/10.1016/j.applthermaleng.2021.117442

[15] Radzai, M.H.M., Yaw, C.T., Lim, C.W., Koh, S.P., Ahmad, N.A. (2021). Numerical analysis on the performance of a radiant cooling panel with serpentine-based design. Energies, 14(16): 4744. https://doi.org/10.3390/en14164744

[16] Jeong, J.W., Mumma, S.A. (2007). Practical cooling capacity estimation model for a suspended metal ceiling radiant cooling panel. Building and Environment, 42(9): 3176-3185. https://doi.org/10.1016/j.buildenv.2006.08.006

[17] Tye-Gingras, M., Gosselin, L. (2011). Investigation on heat transfer modeling assumptions for radiant panels with serpentine layout. Energy and Buildings, 43(7): 1598-1608. https://doi.org/10.1016/j.enbuild.2011.03.004

[18] Shin, M.S., Rhee, K.N., Ryu, S.R., Yeo, M.S., Kim, K.W. (2015). Design of radiant floor heating panel in view of floor surface temperatures. Building and Environment, 92: 559-577. https://doi.org/10.1016/j.buildenv.2015.05.006

[19] Acikgoz, O., Kincay, O. (2015). Experimental and numerical investigation of the correlation between radiative and convective heat-transfer coefficients at the cooled wall of a real-sized room. Energy and Buildings, 108: 257-266. https://doi.org/10.1016/j.enbuild.2015.09.013

[20] Su, L., Li, N., Zhang, X., Sun, Y., Qian, J. (2015). Heat transfer and cooling characteristics of concrete ceiling radiant cooling panel. Applied Thermal Engineering, 84: 170-179. https://doi.org/10.1016/j.applthermaleng.2015.03.045

[21] Zhang, X., Li, N., Su, L., Sun, Y., Qian, J. (2016). Experimental study on the characteristics of non-steady state radiation heat transfer in the room with concrete ceiling radiant cooling panels. Building and Environment, 96: 157-169. https://doi.org/10.1016/j.buildenv.2015.11.006

[22] Yu, G., Xiong, L., Du, C., Chen, H. (2018). Simplified model and performance analysis for top insulated metal ceiling radiant cooling panels with serpentine tube arrangement. Case Studies in Thermal Engineering, 11: 35-42. https://doi.org/10.1016/j.csite.2017.12.006

[23] Oubenmoh, S., Allouhi, A., Mssad, A.A., Saadani, R., Kousksou, T., Rahmoune, M., Bentaleb, M. (2018). Some particular design considerations for optimum utilization of under floor heating systems. Case Studies in Thermal Engineering, 12: 423-432. https://doi.org/10.1016/j.csite.2018.05.010

[24] Mosa, M., Labat, M., Lorente, S. (2019). Constructal design of flow channels for radiant cooling panels. International Journal of Thermal Sciences, 145: 106052. https://doi.org/10.1016/j.ijthermalsci.2019.106052

[25] Qin, S.Y., Cui, X., Yang, C., Jin, L.W. (2021). Thermal comfort analysis of radiant cooling panels with dedicated fresh-air system. Indoor and Built Environment, 30(10): 1596-1608. https://doi.org/10.1177/1420326X20961142

[26] Zhao, Z., Li, Y., Dong, S., Cui, Y., Dai, Z. (2021). An analytic model for transient heat conduction in bi-layered structures with flexible serpentine heaters. Applied Mathematics and Mechanics, 42(9): 1279-1296. https://doi.org/10.1007/s10483-021-2765-9

[27] Xing, D., Li, N. (2022). Reconstruction of hydronic radiant cooling panels: Conceptual design and numerical simulation. Thermal Science and Engineering Progress, 30: 101272. https://doi.org/10.1016/j.tsep.2022.101272

[28] Kim, C.K. (2011). An analytical solution to heat conduction with a moving heat source. Journal of Mechanical Science and Technology, 25: 895-899.

https://doi.org/10.1007/s12206-011-0214-5
[29] Eremin, A.V., Stefanyuk, E.V., Kurganova, O.Y., Tkachev, V.K., Skvortsova, M.P. (2018). A generalized function in heat conductivity problems for multilayer structures with heat sources. Journal of Machinery Manufacture and Reliability, 47: 249-255. https://doi.org/10.3103/S1052618818030056
[30] Rahbari, I., Mortazavi, F., Rahimian, M.H. (2014). High order numerical simulation of non-Fourier heat conduction: An application of numerical Laplace transform inversion. International Communications in Heat and Mass Transfer, 51: 51-58. https://doi.org/10.1016/j.icheatmasstransfer.2013.12.003
[31] ANSI/ASHRAE Standard 55. (1992). Thermal Environmental Conditions for Human Occupancy. https://codehub.building.govt.nz/resources/ashrae-standard-55-1992.
[32] Radiant Cooling Design Manual. Uponor, Inc., USA, 2013. https://www.uponor.com/getmedia/5245da12-094b-42d5-8919-73cd65e129a0/rcdm.pdf?sitename=USA.
[33] Abdulrasool, A.A., Abbas, A.K., Abdullah, W.N. (2023). The cooling effect of blood flow during hyperthermia treatment. Journal of Thermal Biology, 114: 103581. https://doi.org/10.1016/j.jtherbio.2023.103581
[34] Ghasemi, B., Aminossadati, S.M. (2010). Periodic natural convection in a nanofluid-filled enclosure with oscillating heat flux. International Journal of Thermal Sciences, 49(1): 1-9. https://doi.org/10.1016/j.ijthermalsci.2009.07.020

NOMENCLATURE

a	Axial distance
As	Surface area of tube
b	Vertical distance
c	Vertical tube spacing
Cp	Water specific heat capacity taken 4187 in J/kg.K
d	Tube diameter which
G	Pressure drop factor of water
H	Solid box height
hs	Mixed (convection & radiation) heat transfer coefficient of air
K	Thermal conductivity of copper
k	Odd integer number
Ls	Serpentine tube length
Ks	Number of tune turns
n	Integer number
p	Water pressure
R	Tube radius
r	Radial variable,$\sqrt{x^2+y^2}$
T	Solid box temperature
$T*$	Unsteady solid box temperature
T_a	Air temperature
T_{av}	Air operative temperature of the interior room
T_p	Panel average temperature
T_{wi}	Water inlet temperature
T_{tp}	Panel top temperature which is $Twi+(1/a)+x$
T_{bp}	Panel bottom temperature
t	Time
u	Maximum water velocity
$umax$	Maximum water velocity
W	Solid box width
x	Axial axis
y	Vertical axis

Greek symbols

α	Solid box thermal diffusivity
δ	Panel thickness
μ	Eigenvalue with k=1,3,5... etc.
λ	Eigenvalue with n=1,2,3... etc.
Λ	Amplitude of temporal variation which is equal to $2\pi / R$
ν	Water kinematic viscosity
ρ	Water density
θ	Heaviside step function